Journal of Catalysis 278 (2011) 239–245

Contents lists available at ScienceDirect

Journal of Catalysis

journal homepage: www.elsevier.com/locate/jcat

Preferential CO oxidation in a large excess of hydrogen on Pt_3Sn surfaces

C. Dupont [a,b], F. Delbecq [b], D. Loffreda [b], Y. Jugnet [a,*]

[a] Institut de Recherche sur la Catalyse et l'Environnement de Lyon, UMR 5256 CNRS-Université Lyon 1, 2 Avenue Albert Einstein, F-69626 Villeurbanne Cedex, France
[b] Université de Lyon, Institut de Chimie de Lyon, Laboratoire de Chimie, UMR CNRS 5182, Ecole Normale Supérieure de Lyon, 46 Allée d'Italie, F-69364 Lyon Cedex 07, France

ARTICLE INFO

Article history:
Received 21 July 2010
Revised 14 December 2010
Accepted 16 December 2010
Available online 26 January 2011

Keywords:
Bimetallics
CO preferential oxidation
PROX
PM-IRRAS
Operando measurements

ABSTRACT

An experimental evaluation, under realistic conditions, of the catalytic properties of a $Pt_3Sn(1\,1\,1)$ model catalyst in CO oxidation under excess of hydrogen is reported in this study. From a structural point of view, two different surface terminations are available in this alloy, viz. (2×2) and $(\sqrt{3} \times \sqrt{3})R30^\circ$, differing by their tin concentration and Pt–Sn local structural arrangements in the uppermost layers, thus offering specific active sites for the reaction to proceed. In this study, mass spectrometry and polarization modulation infrared reflection absorption spectroscopy measurements (PM-IRRAS) have been performed at near ambient pressure on both surfaces of the alloy and compared to those obtained on $Pt(1\,1\,1)$ used as a reference. The presence of hydrogen promotes the rate of CO oxidation on the three surfaces. The influence of tin is remarkable, increasing the catalytic activity of Pt atoms by one order of magnitude. With the exception of CO, no other species such as formyls or carbonates are observed on the surface by IR spectroscopy in the range of temperature (293–425 K) investigated.

1. Introduction

Pt-based fuel cell anodes are easily poisoned by the presence of CO impurities contained in the combustible hydrogen, and the limitation of this deactivation is still a challenging issue. A first significant removal of CO is performed by the water gas-shift reaction ($CO + H_2O \rightleftharpoons CO_2 + H_2$). However, this is not sufficient for direct application in fuel cells with H_2 still requiring a further purification. The preferential oxidation of CO (PROX) is probably the most efficient process to reduce the CO content to a sufficiently low level (a few ppm) to be compatible with its use in fuel cells [1].

The efficiency of a PROX catalyst depends on its activity in CO oxidation ($CO + 1/2\ O_2 \rightleftharpoons CO_2$), its selectivity with respect to the undesired hydrogen oxidation ($H_2 + 1/2\ O_2 \rightleftharpoons H_2O$), and its resistance to deactivation. Essentially Pt but also other metals, such as Pd, Rh, Ru and Au, supported on various oxides have been proposed and widely tested in the past, as potential selective catalysts for CO preferential oxidation in H_2-rich streams [2,3]. However, as mentioned by Duprez et al., rating the efficiency of these catalysts is not straightforward [4], as a result of too many parameters at stack. Pt-based bimetallic catalysts prepared by adding metals, such as Co, Cu, Ru, Rh and Sn, have been suggested as an alternative solution in a large number of experimental and theoretical investigations whether in electrochemical or gas phase conditions [5–18]. In fact the majority of these bimetallic catalysts exhibit improved efficiency in comparison with pure Pt. For instance, Schubert et al. [7] have compared the catalytic properties of a vulcan supported PtSn catalyst with commercial Pt supported on Al_2O_3. According to this study, PtSn is more active than Pt by two orders of magnitude at a temperature of 80 °C making this catalyst as efficient as Au/Fe_2O_3. In addition, the selectivity of the PtSn catalyst is greatly enhanced compared to Pt, particularly at low temperatures (<80 °C). At some point – regarding the complexity of the reactivity on supported catalysts (nature, size and composition of particles, nature of the support, catalyst preparation) – the study of the reaction on well-defined catalysts is a prerequisite for (a) the characterization of the active site, (b) the understanding of the role of each metallic partner in the alloy performance, (c) the determination of the reaction mechanism or the deactivation process and (d) the structural identification of the reaction intermediates.

Within this context, the performances of the catalytic surfaces of Pt_3Sn alloy for carbon monoxide oxidation have been evaluated and elucidated recently by combining both an experimental and a theoretical approach [19]. Interestingly, $Pt_3Sn(1\,1\,1)$ exhibits two distinct surfaces, viz. the (2×2) and the $(\sqrt{3} \times \sqrt{3})R30^\circ$ differentiated by their surface stoichiometry (Pt_3Sn and Pt_2Sn respectively), and by the local structural arrangement of Pt and Sn atoms in the first surface layers. The comparison of both $Pt_3Sn(1\,1\,1)$ and $Pt(1\,1\,1)$ surfaces under identical conditions has shown that the presence of tin enhances significantly the platinum activity in CO oxidation. Moreover, the extraordinary ability of $Pt_3Sn(1\,1\,1)$ for oxygen dissociation has been demonstrated from first-principles theory, and the mediatory role of tin in this phenomenon has been illustrated by an electronic population analysis. The reaction mechanism for CO oxidation has been addressed, and kinetics has been studied in particular as a function of oxygen

* Corresponding author. Fax: +33 4 72 44 53 99.
E-mail address: yvette.jugnet@ircelyon.univ-lyon1.fr (Y. Jugnet).

0021-9517/$ - see front matter © 2010 Elsevier Inc. All rights reserved.
doi:10.1016/j.jcat.2010.12.012

coverage. The experimental performance in CO oxidation has been found to be structure sensitive, the most active surface of the alloy being the (2×2) termination. Despite these recent efforts aiming at modelling CO oxidation on tailored single crystal surfaces, the performance of $Pt_3Sn(1\,1\,1)$ surfaces towards this reaction under a large excess of hydrogen has not yet been measured.

In this study, we report on the efficiency of the $Pt_3Sn(1\,1\,1)$-(2×2) and -$(\sqrt{3} \times \sqrt{3})R30^\circ$ terminations for PROX under similar conditions, by combining mass spectrometry and polarization modulation infrared spectroscopy (PM-IRRAS). Additional "post-reaction" X-ray photoelectron spectroscopy (XPS) has been performed to check the influence of hydrogen on the electronic state of Pt and Sn surface atoms and to detect a potential segregation of one of the components of the alloy. In the absence of a support, and under reproducible sample preparation conditions, we focus our attention on the influence of hydrogen on the CO oxidation, on the role of tin in presence of hydrogen, on the selectivity of the alloy with respect to carbon monoxide and hydrogen oxidation, on the nature of the surface species and lastly on the influence of the surface structure on the reactivity.

2. Experimental details

The experiments were carried out in a system composed of two main ultra high vacuum (UHV) chambers combined with a UHV-compatible high-pressure cell. The first two chambers are dedicated to sample preparation and XPS, and to high-resolution electron energy loss spectroscopy (HREELS), respectively. The sample preparation chamber is equipped with an ion gun, an electron gun for sample annealing, a quadrupole mass spectrometer, a dual Mg/Al X-ray source and a hemispherical analyser. The base pressure is in the 10^{-10} Torr range.

The high-pressure cell, which has been described previously in detail [20], is a small stainless steel bakeable chamber (1 l) inside an infrared environment allowing vibrational spectroscopy measurements on the catalyst under working conditions. The pressure within the reactor can be varied from the low 10^{-9} Torr range up to one atmosphere. Evacuation of the reactor from high pressures is carried out via an oil free root pump (in the 10^{-3} Torr range) and a turbomolecular pump (in the low 10^{-9} Torr range). The maximum available temperature of the sample is about 475 K under elevated pressures. A K-type thermocouple is in contact with the plate supporting the sample. Gas sampling (reactants and products) for mass spectrometry analysis is operated through a leak valve attached to the reactor.

This cell, which functions as a batch reactor, is equipped with two ZnSe IR windows. PM-IRRAS spectra are obtained from a NEXUS (Thermo Nicolet) Fourier transform infrared spectrometer equipped with a ZnSe polarizer and a 100 MHz photoelastic modulator (PEM-90 from HINDS Instruments). The PM-IRRAS measurements were performed in specular reflection mode under grazing incidence (8° relative to the surface) as described previously [21]. Data were collected at a spectral resolution of 4 cm^{-1}, with 1024 scans co-added. All spectra reported in this paper are normalized to the clean surface spectrum.

The samples were fixed on a Mo plate, which can be transferred as a unit from the UHV preparation chamber to the reactor. The $Pt_3Sn(1\,1\,1)$ sample, a small disc of 0.8 cm diameter, is prepared under UHV conditions by a classical series of ion sputtering (10 min, Ar^+, 2 keV, 10^{-6} Torr), and annealing (20 min to reach segregation equilibrium) until no impurity is detected by XPS. After ion sputtering, a tin depleted surface region is formed due to preferential sputtering of tin relative to Pt. The temperature of the last annealing dictates the atomic structure and composition of the ultimate surface layer [22]: at 600 K, a $(\sqrt{3} \times \sqrt{3})R30^\circ$ reconstruction develops (with 33 at% Sn in the surface layer on top of a Pt enriched second layer), while a (2×2) reconstruction (corresponding to a normally bulk truncated surface with 25 at% Sn in the surface layer) occurs after annealing at 1000–1100 K. Both reconstructions are schematized in Fig. 1.

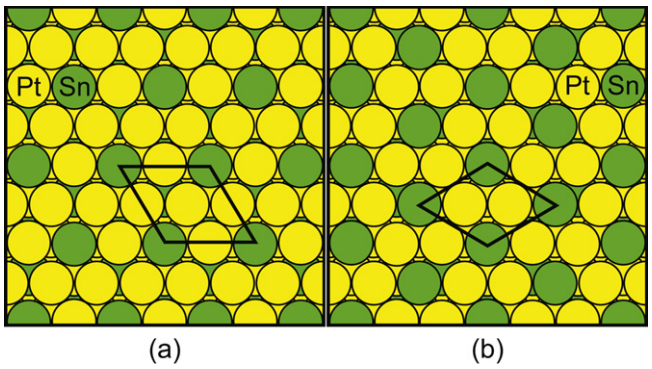

Fig. 1. Scheme of the two surface structures which can be obtained from $Pt_3Sn(1\,1\,1)$-(2×2) depending on the last annealing temperature: (a) $Pt_3Sn(1\,1\,1)$-(2×2) at 1000–1100 K with 25 at% Sn in the topmost layer and (b) $(\sqrt{3} \times \sqrt{3})R30^\circ$ at 600 K with 33 at% Sn in the surface layer.

XPS experiments were performed along the normal to the crystal using the Al Kα X-ray line. On the clean surface, the mean value of tin concentration normalized to that of the (2×2) taken at 25 at% reaches only 17.5 at% in the case of the $(\sqrt{3} \times \sqrt{3})R30^\circ$. Although these values are integrated over the whole depth analysed (a few nm), they clearly indicate a tin depletion in the surface sublayers of the $(\sqrt{3} \times \sqrt{3})R30^\circ$ in agreement with Bardi and coworkers [22]. The $Pt(1\,1\,1)$ used as a reference sample is a small disc of 1 cm diameter. It was also prepared by a series of sputtering and annealing (5 min at 1000 K) cycles with a single intermediate annealing at 900 K under oxygen (10^{-7} Torr) in order to remove residual carbon from the surface.

CO gas (Linde 3.7) was first passed through a molecular sieve (5A 4-8) and then through a liquid nitrogen trap in order to prevent any Ni carbonyl adsorption and further decomposition on the surface. The CO container was equipped with a Ni free valve (Air Liquide). A commercial mixture ("Mélange Crystal" from Air Liquide, N55) of O_2 (1 mol%) in H_2 was used directly without any trapping.

All experiments were conducted following the same procedure: once cleaned and characterized by XPS, the sample is transferred under UHV into the high-pressure cell and an initial PM-IRRAS reference spectrum of the clean surface is recorded at 300 K. 10^{-1} Torr CO plus 100 Torr of the commercial mixture (1 Torr O_2 and 99 Torr of H_2) are then introduced into the reactor. As soon as these gases are in contact with the sample, mass spectra and PM-IRRAS spectra are recorded alternatively as a function of time. Finally, partial pressures of CO, O_2 and CO_2 are calculated from the evolution of masses linked to CO ($m/e = 28$), O_2 ($m/e = 32$) and CO_2 ($m/e = 44$). The direct analysis of water formation ($m/e = 18$) is not possible from a practical point of view owing to the slow diffusion of water into the chamber resulting in an unduly long stabilization time of the water signal. Pure CO, O_2 and CO_2 gases are used for calibrating the mass spectra. The pressure inside the reactor is monitored with a membrane gauge.

3. Results

The catalytic performances of the various surfaces investigated were probed by mass spectrometry, and the analysis of the surface species during the reaction was performed by PM-IRRAS. In addition, the surfaces have been checked by XPS performed before and after reaction.

3.1. Catalytic performances of $Pt_3Sn(1\,1\,1)$ and $Pt(1\,1\,1)$ in PROX conditions

We will start off by describing the behaviour of the $Pt_3Sn(1\,1\,1)$-(2×2) surface under PROX conditions at 380 K, a temperature for which the three surfaces investigated were active in CO oxidation [19], the (2×2) displaying the highest efficiency. The three surfaces will then be compared under similar experimental conditions.

3.1.1. PROX reaction on Pt_3Sn-(2×2) at 380 K

The evolution of the partial pressures of CO, O_2 and CO_2 during the reaction is reported in Fig. 2. Zero reference on the time scale corresponds to the moment when the $(O_2 + H_2)$ mixture is introduced into the chamber and when the heating is started. About 40 min is necessary to reach the fixed temperature due to a strong inertia of our heating system under high-pressure conditions. During this time, 10% of CO is already converted into CO_2 as shown in part 1 of the graph. As a first key remark, these results clearly show that a large excess of H_2 does not prevent CO oxidation on this surface. After about 150 min, almost all the CO is converted into CO_2. For a CO conversion rate lower than 80%, the oxygen pressure decreases slowly (part 2 of the graph) following which a sudden rapid decrease is observed (part 3 of the graph). Regarding the evolution of hydrogen ($m/e = 2$) and water ($m/e = 18$), not quantified (as mentioned previously) and not reported elsewhere in the figure, the data clearly show a constant hydrogen partial pressure in the regions (1) and (2) and no evolution of the residual water signal (only traces exist). In region (3), the water signal starts to increase concomitantly with a small decrease in the hydrogen signal. Combustion of oxygen in region (3) is associated with the oxidation of hydrogen and the formation of water at a high kinetic rate. Hence, $Pt_3Sn(1\,1\,1)$-(2×2) demonstrates catalytic properties which basically fit the requirement for PROX. Indeed, this surface first oxidizes the small amount of CO selectively and then exhibits good catalytic activity for the combustion of purified hydrogen at a reasonably low temperature.

In order to quantify the catalytic performance, activities for CO oxidation in the presence of hydrogen have been calculated following the procedure detailed previously [19]. The activity per surface unit area (mol cm^{-2} s^{-1}) is determined from the slope $\Delta P/\Delta t$ of the curve $P_{CO_2} = f(t)$, with the following formula:

$$A = \frac{1.61 \times 10^{20}}{S} \times \frac{V_{reac}}{T_{reac}} \times \frac{\Delta P}{\Delta t} \quad (1)$$

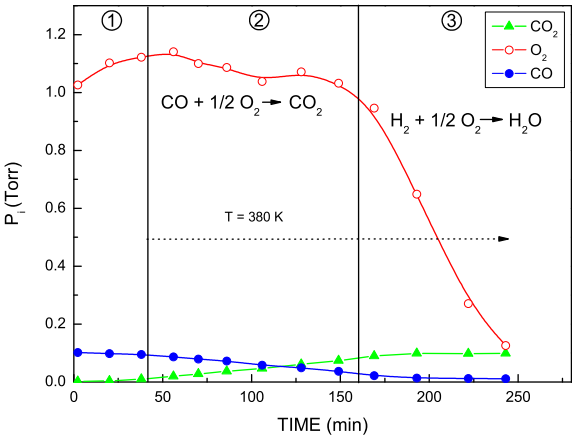

Fig. 2. Evolution of CO_2 (green), CO (blue) and O_2 (red) partial pressures (Torr) as a function of time during CO oxidation in the presence of a large excess of H_2 at 380 K on $Pt_3Sn(1\,1\,1)$-(2×2). 10^{-1} Torr of CO, 1 Torr of O_2 and 99 Torr of H_2 are introduced initially at room temperature. (For interpretation of the references to colour in this figure legend, the reader is referred to the web version of this article.)

A is the activity per surface unit area (mol cm^{-2} s^{-1}), S the sample area (0.5 cm^2 and 0.785 cm^2 for $Pt_3Sn(1\,1\,1)$ and $Pt(1\,1\,1)$ samples, respectively), V_{reac} the volume of the reactor (1.0 l), T_{reac} the reactor temperature (K) and $\Delta P/\Delta t$ the slope of the curve $P_{CO_2} = f(t)$ (Torr min^{-1}). In this work, the activity is systematically determined for conversion rates lower than 50%.

In the following, the activities measured on the $Pt(1\,1\,1)$, $Pt_3Sn(1\,1\,1)$-(2×2) and $Pt_3Sn(1\,1\,1)$-$(\sqrt{3} \times \sqrt{3})R30°$ surfaces at different temperatures under PROX conditions will be discussed in order to determine the relationships between the catalyst performance and its chemical nature, its surface structure and its surface stoichiometry.

3.1.2. Comparison between Pt and PtSn surfaces

The evolution of activity of the three surfaces in CO oxidation in a large excess of hydrogen (PROX) is reported in Fig. 3. For ease of comparison, the activities measured in the absence of hydrogen (COOX) [19] for the same surfaces under identical pressures of CO and O_2 are also reported.

- As previously observed in the absence of hydrogen, the alloy is always more efficient than pure platinum to oxidize CO in the range of temperature investigated (293–425 K). A significant activity is observed at room temperature (5.5×10^{13} mol cm^{-2} s^{-1} and 3.1×10^{13} mol cm^{-2} s^{-1} for the (2×2) and the $(\sqrt{3} \times \sqrt{3})R30°$, respectively). At this temperature, the $Pt(1\,1\,1)$ activity was too low to be evaluated within a reasonable reaction time.
- By increasing the reaction temperature, the activity of the alloy is enhanced by more than one order of magnitude. At 380 K, it is large (73×10^{13} mol cm^{-2} s^{-1} and 67×10^{13} mol cm^{-2} s^{-1} for the (2×2) and $(\sqrt{3} \times \sqrt{3})R30°$ surfaces, respectively) while the performance on $Pt(1\,1\,1)$ is much lower (5.2×10^{13} mol cm^{-2} s^{-1}).
- Let us now compare CO oxidation (COOX) and PROX. At room temperature, the presence of hydrogen slightly improves the performance of the surfaces of the alloy (from 1.4 to 5.5×10^{13} mol cm^{-2} s^{-1} for the (2×2), and from a non-detectable activity to 3.1×10^{13} mol cm^{-2} s^{-1} for the $(\sqrt{3} \times \sqrt{3})R30°$). In contrast, at 380 K the activity gain is globally remarkable ($67–73 \times 10^{13}$ mol cm^{-2} s^{-1}), especially for the $(\sqrt{3} \times \sqrt{3})R30°$ termination (67×10^{13} mol cm^{-2} s^{-1}). For $Pt(1\,1\,1)$, the gain in the presence of hydrogen is less significant at this temperature, because of a globally lower efficiency.

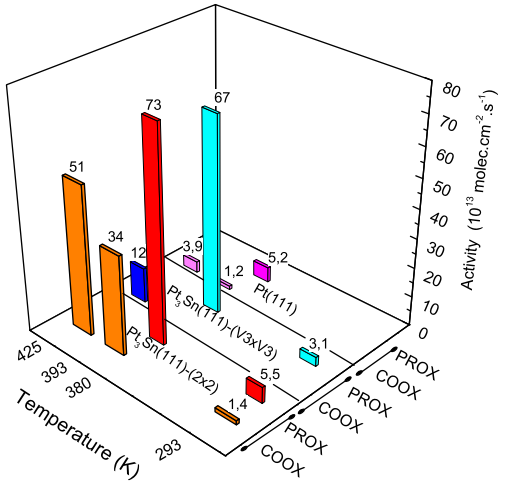

Fig. 3. Evolution of the activity of $Pt_3Sn(1\,1\,1)$-(2×2), $Pt_3Sn(1\,1\,1)-(\sqrt{3} \times \sqrt{3})R30°$ and $Pt(1\,1\,1)$ in CO oxidation and in PROX reaction at different temperatures. The measured values are reported in each case. The experimental conditions are: P(CO) = 0.1 Torr, $P(O_2)$ = 1 Torr and $P(H_2)$ = 99 Torr.

- Finally, the presence of hydrogen cancels the activity difference between the two alloy terminations, in contrast to COOX observations [19]. Whatever the temperature, both PtSn surfaces exhibit a comparable performance with a slight enhancement for the (2×2) termination.

3.2. XPS characterization

In addition to potential structural modifications, adding elevated pressures of gases on a bimetallic surface may also induce preferential segregation of one of the components of the alloy and modify the oxidation states of one or both components. Post-reaction XPS measurements provide additional information although they are limited to irreversible transformations on the surface.

In Table 1, the atomic concentrations of tin and platinum determined on the clean surfaces, after PROX reaction and after CO oxidation (i.e. in the absence of hydrogen), are reported. A small but irreversible tin segregation is observed on both surfaces after PROX reaction, a phenomenon which was not observed after CO oxidation without hydrogen.

The chemical state of Pt and Sn on the two surfaces of the alloy has been studied after CO oxidation and PROX reactions. To start with, the Pt4f and Sn3d signals of the clean surfaces are decomposed into their spin-orbit components. The same curve fitting procedure is then applied on each of the surfaces – (2×2) and $(\sqrt{3} \times \sqrt{3})R30^\circ$ – after CO oxidation and after PROX using the peak resolution parameters determined on the clean surfaces (similar full width at half maximum and same line shape). As shown in Figs. 4 and 5, no chemical shift or broadening which could have been induced by the reaction is observed either on Pt4f or on Sn3d core levels. $Pt4f_{7/2}$ and $Sn3d_{5/2}$ are measured at a binding energy of 71.1 eV (71.05 eV) and 485.6 eV (485.4 eV) on the (2×2) and the $(\sqrt{3} \times \sqrt{3})R30^\circ$ surfaces, respectively. These values are characteristic of Pt and Sn atoms in the $Pt_3Sn(1\,1\,1)$ alloy. The presence of SnO or SnO_2 surface oxides would display new components on Sn3d core levels with a shift of about +1.8 eV and +2.6 eV towards higher binding energy with respect to metallic tin [23–25]. Chemical shifts of +2.0 and +3.7 eV are expected on Pt4f levels in the presence of PtO and PtO_2 oxides [26]. Hence, the formation of stable highly oxidized (SnO, SnO_2, PtO, PtO_2) surface species during the reaction is ruled out, both in COOX and in PROX. This is not so surprising taking into consideration previous results obtained under UHV. In the specific case of Pt–Sn alloys, the oxidation process requires either a high temperature or the use of a strong oxidant. On Sn/Pt(1 1 1) surface alloys [27] and on $Pt_3Sn(1\,1\,1)$ bulk alloy [28], it is known that atomic or molecular oxygen adsorption does not occur at room temperature. Saliba et al. [29] succeeded in oxidizing Pt–Sn surfaces by ozone under UHV conditions; They showed that both surface alloys ((2×2) and $(\sqrt{3} \times \sqrt{3})R30^\circ$) were less reactive than Pt(1 1 1). On $Pt_3Sn(1\,1\,1)$ bulk alloy, Hoheisel et al. identified a two-dimensional tin oxygen layer obtained only after an exposure to 9000 L O_2 (1 L = 10^{-6} Torr × 1 s) at a temperature of 770 K [28]. In the present study, under high-pressure and relatively low-temperature conditions, we reject the possibility of the formation of stable heavily oxidized PtSn; however, one cannot exclude the formation of PtO_x or more probably SnO_x ($x < 1$) isolated suboxide islands, as supported by theoretical results [39]. Unfortunately, the picture regarding the formation of such entities cannot be clear-cut yet, due to the lack of resolution and also to the lack of surface sensitivity of a standard non-monochromatized XPS apparatus.

Table 1
Evolution of the tin concentration (at%) on $Pt_3Sn(1\,1\,1)$-(2×2) and $Pt_3Sn(1\,1\,1)$-$(\sqrt{3} \times \sqrt{3})R30^\circ$ surfaces determined by XPS under UHV conditions after PROX reaction. For comparison, results obtained after CO oxidation reaction are reported.

Surface	$Pt_3Sn(1\,1\,1)$-(2×2) (%)	$Pt_3Sn(1\,1\,1)$-$(\sqrt{3} \times \sqrt{3})R30^\circ$ (%)
Clean	25.3	17.5
COOX	25.4	17.8
PROX	27.2	20.8

3.3. Infrared spectroscopic measurements

PM-IRRAS spectra recorded in the whole wavenumber range 400–4000 cm^{-1} for the three surfaces during PROX reaction are reported in Fig. 6. It is important to note that except for the ν (CO) stretching frequency, no other vibrational band assigned to other surface species, such as carbonates, formates or hydroxyls, has been detected. This is fully compatible with previous

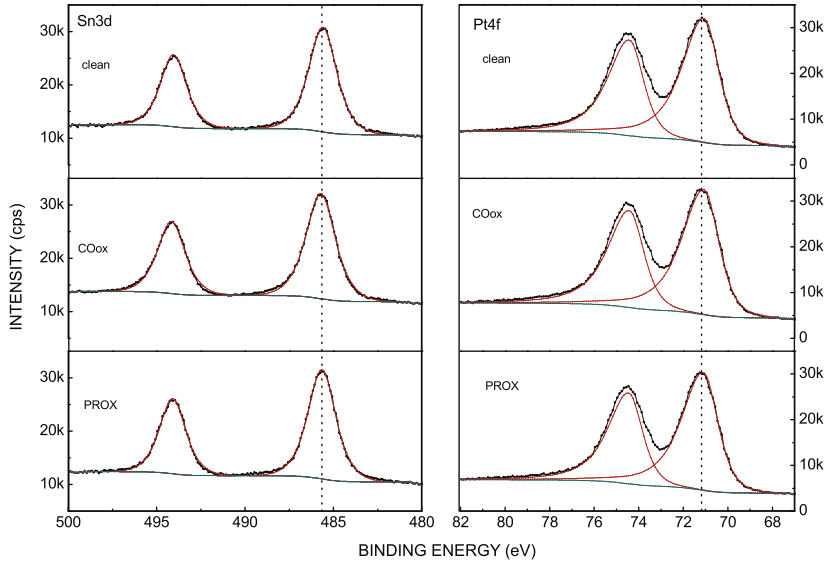

Fig. 4. Pt4f and Sn3d core levels measured on $Pt_3Sn(1\,1\,1)$-(2×2) immediately after cleaning, after CO oxidation and after PROX. Following a Shirley background subtraction, Sn3d and Pt4f spin-orbit components are fitted with gaussian lorentzian and asymmetric gaussian lorentzian profiles, respectively.

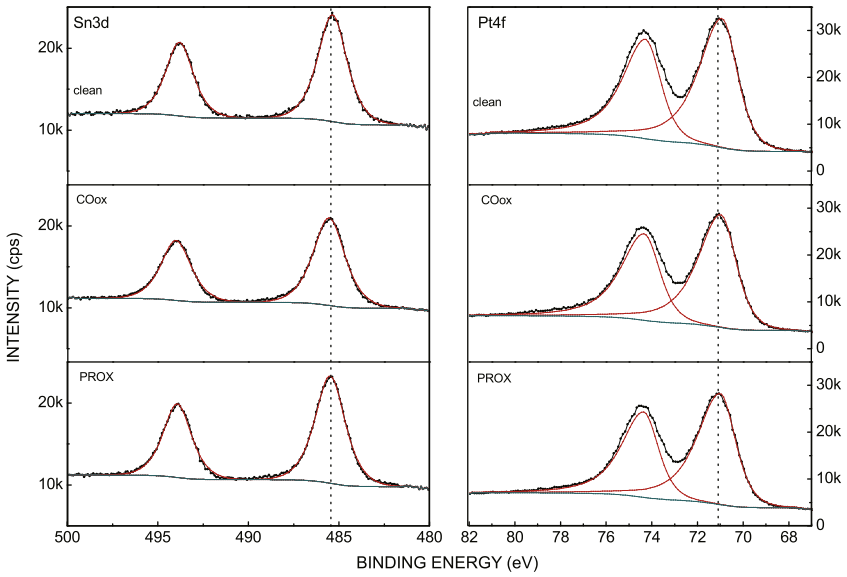

Fig. 5. Pt4f and Sn3d core levels measured on $Pt_3Sn(1\,1\,1)$-$(\sqrt{3} \times \sqrt{3})R30^\circ$ immediately after cleaning, after CO oxidation and after PROX. Following a Shirley background subtraction, Pt4f and Sn3d spin-orbit components are fitted with asymmetric gaussian lorentzian and gaussian lorentzian, respectively.

measurements in an electrochemical environment for CO oxidation on $Pt_3Sn(1\,1\,1)$ [30]. In the following, only the CO stretching vibrational band will be discussed. For each surface, spectra have been recorded under 0.1 Torr CO at room temperature (a), then after the addition of 100 Torr of the mixture (O_2/H_2: 1/100) at room temperature (b), during the heating procedure (c) and finally after a few hours of reaction at 380 K (d).

As noted previously [21], under CO pressure alone the signal is much more intense on Pt(1 1 1) than on the two surfaces of the alloy. This can be explained by the small size of the PtSn sample, by the reduction of the number of Pt atoms in its topmost layer and by its lower CO affinity compared to Pt(1 1 1). In each case CO is linearly adsorbed on top of a Pt atom.

Adding the (O_2/H_2) mixture to CO at 300 K does not induce any perturbation on Pt(1 1 1): no shifting of the ν(CO) band which remains at 2096 cm^{-1}, and no loss in intensity (see Fig. 6b). It must

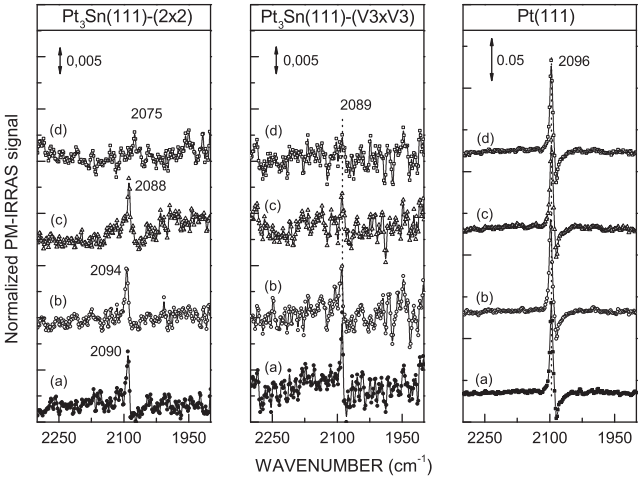

Fig. 6. Evolution of the PM-IRRAS spectra during CO oxidation in the presence of H_2 at 380 K on $Pt_3Sn(1\,1\,1)$-(2×2), $Pt_3Sn(1\,1\,1)$-$(\sqrt{3} \times \sqrt{3})R30^\circ$ and Pt(1 1 1) for comparison. All spectra are recorded under the following static conditions: (a) 10^{-1} Torr CO at room temperature, (b) same as (a) plus 1 Torr O_2 +99 Torr H_2 at room temperature, (c) same as (b) about 40 min after starting the heating procedure and $T = 370$ K, (d) same as (b) after 2–3 h at 380 K (170, 110 and 215 min) on ($Pt_3Sn(1\,1\,1)$-(2×2), $Pt_3Sn(1\,1\,1)$-$(\sqrt{3} \times \sqrt{3})R30^\circ$ and Pt(1 1 1) respectively.)

be recalled that under such conditions, no CO_2 was produced on Pt(1 1 1) (see Fig. 3). With the $Pt_3Sn(1\,1\,1)$ alloy the situation is different since both terminations are already active for the CO oxidation step at room temperature. On the (2×2) surface, the ν(CO) band is slightly blue-shifted to 2094 cm^{-1}, while maintaining a constant intensity. In contrast, no shift is observed on the $Pt_3Sn(1\,1\,1)$-$(\sqrt{3} \times \sqrt{3})R30^\circ$ surface, but the introduction of 100 Torr of O_2/H_2 leads to an intensity loss of more than 50% of the ν(CO) band. This can be attributed to a partial desorption of CO induced by the ($O_2 + H_2$) mixture on the $(\sqrt{3} \times \sqrt{3})R30^\circ$ surface, which is not observed on the (2×2). This is in agreement with the higher adsorption energy calculated for CO on $Pt_3Sn(1\,1\,1)$-(2×2) [19] and with the differences of behaviour between the two terminations already observed during the coadsorption of CO with O_2 [21]. In that study, it was shown that oxygen alone (1 Torr) added to CO (0.1 Torr) at room temperature, induced an almost imperceptible blue-shift of the ν(CO) band on the two terminations of the alloy and a partial desorption of CO only in the case of the $(\sqrt{3} \times \sqrt{3})R30^\circ$ surface. The loss of intensity of the ν(CO) band is accompanied by some band broadening which could be due to a structural reorganization of the surface induced by the high pressure of hydrogen. Structural studies under such conditions would be very helpful to confirm this hypothesis.

PM-IRRAS spectra were then measured during the heating process, once the temperature reached 370 K (Fig. 6c) and after a few hours at 380 K (Fig. 6d). At 370 K, no spectral evolution is observed on Pt(1 1 1). The same observation is valid even after 215 min at 380 K. Under such conditions, the conversion rate is less than 20% (see Fig. 3) since it is inhibited by the CO site blocking effect on Pt atoms rendering oxygen adsorption and further CO oxidation difficult. The very strong interaction between CO and Pt even at 380 K under high pressure of hydrogen is obviously the cause of the low activity measured for Pt(1 1 1) in PROX, CO desorption appearing as the rate determining step of this reaction. As described below, the behaviour of the alloy with respect to temperature is different.

On the (2×2) surface, once the temperature reaches 370 K, the ν(CO) stretching band is now red-shifted to 2088 cm^{-1} without any loss of intensity. The CO conversion rate is estimated at about 15%. Other spectra, not shown here, have been recorded at 380 K for CO conversion rates of up to 50%, and they do not display further modification. After 170 min at 380 K, an important decrease in the

intensity of the ν(CO) associated with a red shift of 13 cm^{-1} is observed (see Fig. 6d). The poor signal to noise ratio is attributed to a very small CO coverage. At this point, almost all CO has been converted.

The catalytic behaviour of the $(\sqrt{3} \times \sqrt{3})R30^\circ$ termination is basically different. In contrast to the (2×2) observations, increasing the temperature to 370 K results in a large decrease in intensity without any shift of the ν(CO) band. CO conversion at this juncture is rather low. After 110 min at 380 K, the ν(CO) band has almost vanished while the reaction is still running with a conversion rate of 50% (Fig. 6d).

The results at 380 K, under PROX conditions, can briefly be summarized as follows: the relative inefficiency of Pt(1 1 1) is related to a high coverage of too strongly bonded CO which cannot be removed either by oxygen or by hydrogen. On the Pt_3Sn(1 1 1)-(2×2) surface, which is the most efficient one for CO oxidation in the presence or absence of hydrogen, the active CO species is the top CO one (ν(CO) = 2088 cm^{-1}) since it disappears when the CO oxidation is complete. Once all the CO has been oxidized the hydrogen oxidation can start. The situation for the $(\sqrt{3} \times \sqrt{3})R30^\circ$ termination is not as obvious since under reaction conditions almost no CO is observed. Either this really corresponds to a very low CO coverage owing to partial desorption induced by O_2 and H_2 or also by temperature, or it is adsorbed in such a way that it does not fulfil the IR surface selection rules anymore. In the first case, we would have expected a shift of the ν(CO) band with decreasing CO coverage, which is not observed here. In the second case, some restructuring would have occurred in the surface layers.

3.4. Discussion

Over the years, several experimental groups have tackled the fundamental question of explaining the specific activity of pure platinum catalysts or a few platinum-based bimetallic catalytic materials towards the preferential oxidation of carbon monoxide in presence of hydrogen. Different explanations and points of view have been addressed in the literature so far, without clearly elucidating the experimental observations. In the following section, we will briefly recall the proposed scenarios and discuss to what extent our new measurements on PtSn alloy surfaces support the corresponding assumptions.

Regarding the measurements for carbon monoxide oxidation alone on Pt_3Sn(1 1 1) surface terminations, tin exhibits a promoting effect that is linked to a significant increase in catalytic activity with respect to pure platinum, effect which is maintained in the presence of a large excess of hydrogen. This supports previous experimental studies for PROX on Pt_3Sn alloy [7,31]. The gain in PROX activity is unequivocally more pronounced for the $(\sqrt{3} \times \sqrt{3})R30^\circ$ termination. The hydrogen pressure not only increases the catalytic activity of the Pt_3Sn(1 1 1) surfaces, it also lifts PROX performances to similar levels irrespective of surface tin content. In short, both Sn and H_2 contribute to the enhancement of the catalytic activity in CO oxidation making the Pt_3Sn catalyst very promising for PROX. These observations raise several fundamental questions related to the nature of the catalytic surface during the reaction in terms of composition and morphology, and to the nature of the reaction mechanism and intermediates.

One track to explore is the XPS measurement of the tin distribution before and after reaction on both Pt_3Sn(1 1 1) surface terminations. Clearly these XPS observations show a small segregation of tin only after PROX. The tempting conclusion would be to assign this phenomenon to the hydrogen pressure, in the light of previous experimental studies on bimetallics evoking the possibility of a preferential segregation. Such reversible structural modulations of alloys under various reactants under pressure have been demonstrated previously [32–34]. The reasons that could explain this segregation are numerous. Among the most likely assumptions, the hydrogen pressure might induce a significant content of surface and subsurface atomic hydrogen that could force the bimetallic system to reorganize and exhibit a deep restructuring. This might have a non-negligible consequence in the simultaneous presence of oxygen, especially regarding the formation of surface tin oxides SnO_x, which is often evoked for various conditions in the literature, but not detected by post-reaction XPS. For instance, under a pressure of pure oxygen around 10^{-2} Torr, in the range 380–425 K, Jerdev et al. [35] studied the oxidation kinetics of the same surfaces and showed that oxygen accumulation proceeds by oxidation of tin forming quasi-metallic (SnO_x, $0 < x < 1$) and oxidic (SnO_x, $1 < x < 2$) species. They also showed that the oxidation of these alloys resulted in a disruption of the ordered alloy surfaces. In the present work, the maximum temperature is 380 K, and in the presence of a high hydrogen pressure, one can expect that chemisorbed CO will probably limit the oxidation of the alloy. Although the formation of some SnO_x units on the surface cannot be excluded completely, we rather think that chemisorbed atomic oxygen is the most active species for COOX. To summarize, the assumption of a tin segregation could reconcile our results regarding the structure sensitivity observed during COOX and absent during PROX (cf. Fig. 3). Although such an argument is attractive, only fine structural studies could confirm this hypothesis.

The change of the reaction mechanism between COOX and PROX is the second key track that could explain the discrepancies in performance. Our previous investigation into COOX on the Pt_3Sn(1 1 1) surface terminations combining kinetic measurements and density functional theory calculations has given rise to substantial arguments in favour of a reaction mechanism mediated by surface atomic oxygen [19]. In the range of temperatures considered, Sn is predominantly in a metallic state, which does not allow the chemisorption of carbon monoxide. The major conclusion is the outstanding ability of tin-based active sites for the dissociation of molecular oxygen with respect to pure platinum catalysts. For PROX, the picture is far from being as simple as the situation for COOX. A suitable approach aiming at identifying the surface species formed during PROX is the spectroscopic measurement by PM-IRRAS throughout the reaction. Unequivocally, only chemisorbed CO has been detected so far both for COOX and PROX catalytic tests. This fact does not really support the assumptions suggesting a reaction mechanism mediated by hydroxyl (OH) or hydroperoxyl (OOH) surface species [14,36,37], although a minute content that is barely detectable can never be ruled out. Even worse, the absence of any significant vibrational shift of the ν(CO) band for either COOX or PROX is a strong argument in favour of a very weak coverage of hydroxylated or carbonate species, since these species would surely be responsible for vibrational dynamic coupling. In addition, the absence of any shift also supports the argument of a surface weakly covered by tin oxides, in agreement with a UHV study [27]. Hence, our spectroscopic results for PROX seem to suggest a reaction mechanism that is different from frequently evoked assumptions [14]. To our mind, the synergy between the catalyst morphology, its composition, and the surface coverage of reactants, imposed by the operating conditions, would exclude the formation of water and hydroxylated species in the first reaction step. The previously evoked formation of tin oxide islands induced by the presence of hydrogen on the catalytic surface is also an argument against the formation of OH and OOH species. The carbon monoxide oxidation would then occur preferentially on non-oxidized domains where the active sites would be almost exclusively occupied by CO and atomic oxygen, due to their stronger chemisorption energy with respect to hydrogen [19,38–41]. This partially satisfactory explanation is at least fully compatible with our kinetic measurements that have undeniably shown the outstanding ability of Pt_3Sn(1 1 1) surface terminations for PROX.

4. Conclusion

In the present study, we have shown that the $Pt_3Sn(1\,1\,1)$ alloy surfaces are always more active than the pure Pt(1 1 1) surface, both in the absence (COOX) and in the presence (PROX) of hydrogen. By comparing COOX and PROX reactions under identical conditions, we have demonstrated unambiguously the promoting effect of hydrogen on carbon monoxide oxidation, on all the investigated surfaces – $Pt_3Sn(1\,1\,1)$-(2×2), $Pt_3Sn(1\,1\,1)$-$(\sqrt{3} \times \sqrt{3})R30^\circ$ and Pt(1 1 1).

On the basis of the experimental XPS observations of the catalyst composition before and after reaction and of the identification of the surface species by PM-IRRAS, we have come to the following conclusions. Regarding the modifications of the catalyst under PROX operating conditions, the observed segregation of tin encourages us to think that the PtSn bimetallic system undergoes a deep restructuring controlled by oxygen and hydrogen pressures. Our moderate oxidation conditions open up the question of the formation and stability of tin oxides. Concerning the reaction mechanism during the carbon monoxide oxidation, the spectroscopic measurements do not support the hypothesis of a mechanism mediated by hydroxylated species.

Work is still in progress to solve the critical question of the nature of the active phase in carbon monoxide oxidation reactions, a question that is highly debated in the literature (surface oxide versus chemisorbed atomic oxygen) [42,43]. Finally, our results appeal for fine structural studies by scanning tunnelling microscopy and grazing incidence X-ray diffraction measurements under operating conditions.

Acknowledgment

The authors thank U. Bardi from University of Firenze for supplying the $Pt_3Sn(1\,1\,1)$ crystal and N. S. Prakash for critical reading of the manuscript.

References

[1] G.D. Holladay, J. Hu, Y. Wang, Catal. Today 139 (2009) 244.
[2] E.D. Park, D. Lee, H.C. Lee, Catal. Today 139 (2009) 280.
[3] Y.H. Kim, E.D. Park, H.C. Lee, D. Lee, K.H. Lee, Catal. Today 146 (2009) 253.
[4] N. Bion, F. Epron, M. Moreno, F. Marino, D. Duprez, Top. Catal. 51 (2008) 76.
[5] T. Komatsu, A. Tamura, J. Catal. 258 (2008) 306.
[6] G. Avgouropoulos, T. Ioannides, Appl. Catal. B. Environ. 56 (2005).
[7] M.M. Schubert, M.J. Kahlich, G. Feldmeyer, M. Huttner, S. Hackenberg, H.A. Gasteiger, R.J. Behm, Phys. Chem. Chem. Phys. 3 (2001) 1123.
[8] T.E. Shubina, M.T.M. Koper, Electrochim. Acta 47 (2002) 3621.
[9] M.T.M. Koper, T.E. Shubina, R.A. van Santen, J. Phys. Chem. B 106 (2001) 686.
[10] P. Liu, A. Logadottir, J.K. Norskov, Electrochim. Acta 48 (2003) 3731.
[11] V.R. Stamenković, M. Arenz, B.B. Blizanac, K.J.J. Mayrhofer, P.N. Ross, N.M. Marković, Surf. Sci. 576 (2005) 145.
[12] H.A. Gasteiger, N.M. Marković, P.N. Ross, J. Phys. Chem. 99 (1995) 8945.
[13] H.A. Gasteiger, N.M. Marković, P.N. Ross, J. Phys. Chem. 99 (1995) 16757.
[14] S. Alayoglu, A.U. Nilekar, M. Mavrikakis, B. Eichhorn, Nature Mater. 7 (2008) 333.
[15] S. Alayoglu, B. Eichhorn, J. Am. Chem. Soc. 130 (2008) 17479.
[16] B.N. Grgur, G. Zhuang, N.M. Marković, P.N. Ross, J. Phys. Chem. B 101 (1997) 3910.
[17] J.H. Wee, K.Y. Lee, J. Power Sour. 157 (2006) 128.
[18] S. Zhou, G.S. Jackson, B. Eichorn, Adv. Funct. Mater. 17 (2007) 3099.
[19] C. Dupont, Y. Jugnet, F. Delbecq, D. Loffreda, J. Catal. 273 (2010) 211.
[20] L.J. Shorthouse, Y. Jugnet, J.C. Bertolini, Catal. Today 70 (2001) 33.
[21] C. Dupont, D. Loffreda, F. Delbecq, F.S. Aires, E. Ehret, Y. Jugnet, J. Phys. Chem. C 112 (2008) 10862.
[22] W.C.A.N. Ceelen, A.W.D. van der Gon, M.A. Reijme, H.H. Brongersma, I. Spolveri, A. Atrei, U. Bardi, Surf. Sci. 406 (1998) 264.
[23] A.F. Lee, R.M. Lambert, Phys. Rev. B 58 (1998) 4156.
[24] M. Batzill, D.E. Beck, D. Jerdev, B.E. Koel, J. Vac. Sci. Technol. A 19 (2001) 1953.
[25] M. Batzill, J. Kim, D.E. Beck, B.E. Koel, Phys. Rev. B 69 (2004) 165403.
[26] A.S. Aricò, A.K. Shukla, H. Kim, S. Park, M. Min, V. Antonucci, Appl. Surf. Sci. 172 (2001).
[27] M.T. Paffett, S.C. Gebhard, R.G. Windham, B.E. Koel, J. Phys. Chem. 94 (1990) 6831.
[28] M. Hoheisel, S. Spiller, W. Heiland, A. Atrei, U. Bardi, G. Rovida, Phys. Rev. B 66 (2002) 165416.
[29] N.A. Saliba, Y.L. Tsai, B.E. Koel, J. Phys. Chem. B 103 (1999) 1532.
[30] V.R. Stamenković, M. Arenz, C.A. Lucas, M.E. Gallagher, P.N. Ross, N.M. Marković, J. Am. Chem. Soc. 125 (2003) 2736.
[31] H.A. Gasteiger, N.M. Markovic, P.N. Ross, Catal. Lett. 36 (1996) 1.
[32] A. Baraldi, D. Giacomello, L. Rumiz, M. Moretuzzo, S. Lizzit, F.B. de Mongeot, G. Paolucci, G. Comelli, R. Rosei, B.E. Nieuwenhuys, U. Valbusa, M.P. Kiskinova, J. Am. Chem. Soc. 127 (2005) 5671.
[33] T. Ma, Q. Fu, H.-Y. Su, H.-Y. Liu, Y. Cui, Z. Wang, R.-T. Mu, W.-X. Li, X.-H. Bao, ChemPhysChem 10 (2009) 1013.
[34] F. Tao, M.E. Grass, Y. Zhang, D.R. Butcher, J.R. Renzas, Z. Liu, J.Y. Chung, B.S. Mun, M. Salmeron, G.A. Somorjai, Science 322 (2008) 932.
[35] D.I. Jerdev, B.E. Koel, Surf. Sci. 492 (2001) 106.
[36] T. Jacob, W.A.G. III, ChemPhysChem 7 (2006) 992.
[37] J.A. Keith, G. Jerkiewicz, T. Jacob, ChemPhysChem 11 (2010) 2779.
[38] C. Dupont, D. Loffreda, F. Delbecq, Y. Jugnet, J. Phys. Chem. C 111 (2007) 8254.
[39] C. Dupont, Y. Jugnet, F. Delbecq, D. Loffreda, J. Chem. Phys. 130 (2009) 124716.
[40] J. Fearon, G.W. Watson, J. Mater. Chem. 16 (2006) 1989.
[41] F. Vigne, J. Haubrich, D. Loffreda, P. Sautet, F. Delbecq, J. Catal. 275 (2010) 129.
[42] F. Gao, Y. Wang, D.W. Goodman, J. Phys. Chem. 114 (2010) 6874.
[43] R. van Rijn, O. Balmes, R. Felici, J. Gustafson, D. Wermeille, R. Westerstrom, E. Lundgren, J.W.M. Frenken, J. Phys. Chem. 114 (2010) 6875.